Newtonian Flow in

Converging-Diverging Capillaries

Taha Sochi[*]

December 13, 2012

[*]Imaging Sciences & Biomedical Engineering, King's College London, The Rayne Institute, St Thomas' Hospital, London, SE1 7EH, UK. Email: taha.sochi@kcl.ac.uk.

Contents

List of Figures

List of Tables

3

Abstract

The one-dimensional Navier-Stokes equations are used to derive analytical expressions for the <mark>relation between pressure and volumetric flow rate in capillaries of five different converging-diverging axisymmetric geometries for Newtonian fluids.</mark> The results are compared to previously-derived expressions for the same geometries using the lubrication approximation. The results of the one-dimensional Navier-Stokes are identical to those obtained from the lubrication approximation within a non-dimensional numerical factor. The derived flow expressions have also been validated by comparison to <mark>numerical solutions obtained from discretization with numerical integration.</mark> Moreover, they have been certified by testing the convergence of solutions as the converging-diverging geometries approach the limiting straight geometry.

Keywords: Fluid dynamics; One-dimensional Navier-Stokes; Converging-diverging capillaries; Newtonian fluids.

1 Introduction

Modeling the flow through capillaries of converging-diverging geometries is an important subject and has many scientific and industrial applications. Moreover, it is required for modeling viscoelasticity, yield-stress and the flow of Newtonian and non-Newtonian fluids through porous media [1–8].

There are many previous attempts to model the flow through capillaries of various geometries. However, they either apply to tubes of regular cross sections [9, 10] or deal with very special cases. Most these studies use numerical meshing techniques such as finite difference and spectral methods to obtain numerical results. Some examples of these attempts are Kozicki *et al.* [11], Miller [12], Oka [13], Williams and Javadpour [14], Phan-Thien *et al.* [15, 16], Lahbabi and Chang [17], Burdette *et al.* [18], Pilitsis *et al.* [19, 20], James *et al.* [21], Talwar and Khomami [22], Koshiba *et al.* [23], Masuleh and Phillips [24], and Davidson *et al.* [25].

In this article we use the one-dimensional Navier-Stokes equations, which are widely used to describe axisymmetric flows in large vessels, to derive analytical expressions for the flow of Newtonian fluids in tubes of five axisymmetric converging-diverging geometries, some of which are schematically depicted in Figure 1, and compare our results to previously-derived expressions using the lubrication approximation [26]. Other validation tests have also been presented.
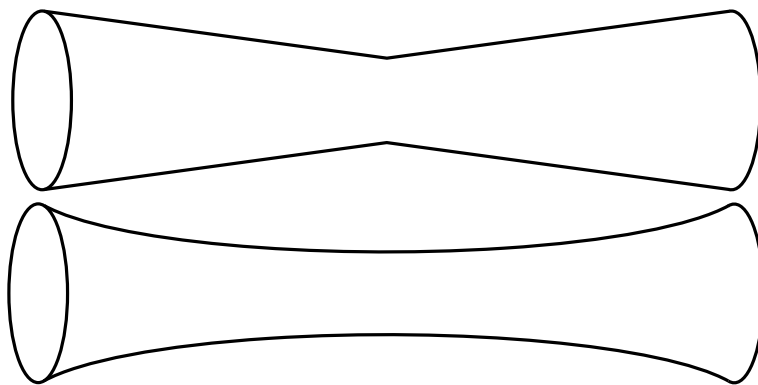

Figure 1: Profiles of converging-diverging axisymmetric capillaries.

The widely-used one-dimensional form of the Navier-Stokes equations to describe the flow in a tube of length L where its axis is aligned with the x axis and its midpoint is at $x = 0$ is given by the following continuity and momentum balance relations respectively assuming negligible gravitational body forces [27–39]

$$\frac{\partial A}{\partial t} + \frac{\partial Q}{\partial x} = 0 \qquad t \geq 0, \; x \in \left[-\frac{L}{2}, \frac{L}{2}\right] \qquad (1)$$

$$\frac{\partial Q}{\partial t} + \frac{\partial}{\partial x}\left(\frac{\alpha Q^2}{A}\right) + \frac{A}{\rho}\frac{\partial p}{\partial x} + \kappa\frac{Q}{A} = 0 \qquad t \geq 0, \; x \in \left[-\frac{L}{2}, \frac{L}{2}\right] \qquad (2)$$

In these equations, A is the tube cross sectional area, t is time, Q ($= A\bar{u}$ with $\bar{u}$ being the mean axial fluid speed) is the volumetric flow rate, x is the axial coordinate along the tube, α ($= \frac{\int u^2 dA}{A\bar{u}^2}$ with u being the local axial fluid speed) [29, 33, 40] is the correction factor for axial momentum flux, ρ is the fluid mass density, p is the pressure, and κ is a viscosity friction coefficient which is given by $\kappa = \frac{2\pi\alpha\mu}{\rho(\alpha-1)}$ [35, 37] with μ being the fluid dynamic viscosity. This model is considered one-dimensional due to the fact that the θ dependency of a cylindrically-coordinated capillary is ignored due to the axisymmetric flow assumption while the r dependency is neglected because of the simplified consideration of the flow profile within a lumped parameter which is the momentum correction factor. Therefore, the only explicitly-considered dependency is the dependency in the flow direction, x.

For steady flow, the time terms are zero, and hence Q as a function of x is constant according to the continuity equation. The momentum equation then becomes

$$\frac{\partial}{\partial x}\left(\frac{\alpha Q^2}{A}\right) + \frac{A}{\rho}\frac{\partial p}{\partial x} + \kappa\frac{Q}{A} = 0 \qquad (3)$$

that is

$$\frac{\partial p}{\partial x} = -\frac{\rho}{A}\frac{\partial}{\partial x}\left(\frac{\alpha Q^2}{A}\right) - \kappa\rho\frac{Q}{A^2} = \frac{\rho\alpha Q^2}{A^3}\frac{\partial A}{\partial x} - \kappa\rho\frac{Q}{A^2} \tag{4}$$

For a flow in the positive x direction, the pressure gradient is negative and hence

$$p = \int_X \kappa\rho\frac{Q}{A^2}dx - \int_X \frac{\rho\alpha Q^2}{A^3}\frac{\partial A}{\partial x}dx \tag{5}$$

$$= \int_X \kappa\rho\frac{Q}{A^2}dx - \int_A \frac{\rho\alpha Q^2}{A^3}dA \tag{6}$$

$$= \kappa\rho Q\int_X \frac{dx}{A^2} - \rho\alpha Q^2\int_A \frac{dA}{A^3} \tag{7}$$

that is

$$p = \kappa\rho Q\int_{x=-L/2}^{L/2}\frac{dx}{A^2} + \frac{\rho\alpha Q^2}{2}\left[\frac{1}{A^2}\right]_{x=-L/2}^{L/2} \tag{8}$$

Due to the tube symmetry with respect to $x = 0$

$$\int_{x=-L/2}^{L/2}\frac{dx}{A^2} = 2\int_{x=0}^{L/2}\frac{dx}{A^2} \tag{9}$$

and

$$\left[\frac{1}{A^2}\right]_{x=-L/2}^{L/2} = 0 \tag{10}$$

Hence

$$p = 2\kappa\rho Q\int_{x=0}^{L/2}\frac{dx}{A^2} \tag{11}$$

This expression is dimensionally consistent.

1.1   Conical Tube
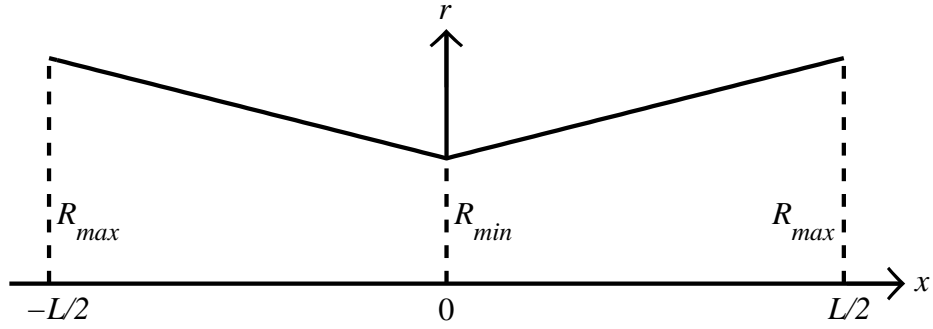
Figure 2: Schematic representation of the radius of a conically shaped converging-diverging capillary as a function of the distance along the tube axis.

For a tube of conical profile, depicted in Figure 2, the radius r as a function of the axial distance x is given by

$$r(x) = a + b|x| \qquad -L/2 \leq x \leq L/2 \tag{12}$$

where

$$a = R_{min} \qquad \text{and} \qquad b = \frac{2(R_{max} - R_{min})}{L} \tag{13}$$

Hence, Equation 11 becomes

$$p = 2\kappa\rho Q \int_{x=0}^{L/2} \frac{dx}{A^2} = 2\kappa\rho Q \int_{x=0}^{L/2} \frac{dx}{\pi^2 (a + bx)^4} \tag{14}$$

$$= -2\kappa\rho Q \left[\frac{1}{3\pi^2 b (a + bx)^3} \right]_0^{L/2} \tag{15}$$

$$= -2\kappa\rho Q \left[\frac{1}{3\pi^2 \frac{2(R_{max}-R_{min})}{L} \left(R_{min} + \frac{2(R_{max}-R_{min})}{L} x \right)^3} \right]_0^{L/2} \tag{16}$$

$$= -2\kappa\rho Q \left[\frac{L}{6\pi^2(R_{max} - R_{min})R_{max}^3} - \frac{L}{6\pi^2(R_{max} - R_{min})R_{min}^3} \right] \tag{17}$$

that is

$$p = \frac{\kappa\rho QL}{3\pi^2(R_{max} - R_{min})} \left[\frac{1}{R_{min}^3} - \frac{1}{R_{max}^3} \right] \tag{18}$$

1.2   Parabolic Tube
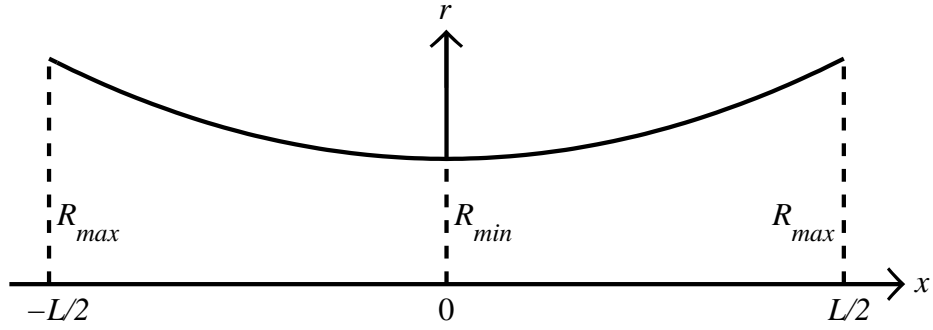
Figure 3: Schematic representation of the radius of a converging-diverging capillary with a parabolic profile as a function of the distance along the tube axis.

For a tube of parabolic profile, depicted in Figure 3, the radius is given by

$$r(x) = a + bx^2 \qquad -L/2 \leq x \leq L/2 \tag{19}$$

where

$$a = R_{min} \qquad \text{and} \qquad b = \left(\frac{2}{L}\right)^2 (R_{max} - R_{min}) \tag{20}$$

Therefore, Equation 11 becomes

$$p = 2\kappa\rho Q \int_{x=0}^{L/2} \frac{dx}{A^2} = 2\kappa\rho Q \int_{x=0}^{L/2} \frac{dx}{\pi^2 (a + bx^2)^4} \tag{21}$$

$$= \frac{2\kappa\rho Q}{\pi^2} \left[\frac{x}{6a\left(a+bx^2\right)^3} + \frac{5x}{24a^2\left(a+bx^2\right)^2} + \frac{5x}{16a^3\left(a+bx^2\right)} + \frac{5\arctan\left(x\sqrt{\frac{b}{a}}\right)}{16a^{7/2}\sqrt{b}} \right]_0^{L/2} \tag{22}$$

that is

$$p = \frac{\kappa\rho QL}{2\pi^2} \left[\frac{1}{3R_{min}R_{max}^3} + \frac{5}{12R_{min}^2R_{max}^2} + \frac{5}{8R_{min}^3R_{max}} + \frac{5\arctan\left(\sqrt{\frac{R_{max}-R_{min}}{R_{min}}}\right)}{8R_{min}^{7/2}\sqrt{R_{max}-R_{min}}} \right] \tag{23}$$

1.3   Hyperbolic Tube

For a tube of hyperbolic profile, similar to the profile in Figure 3, the radius is given by

$$r(x) = \sqrt{a+bx^2} \qquad -L/2 \le x \le L/2 \qquad a,b > 0 \tag{24}$$

where

$$a = R_{min}^2 \qquad \text{and} \qquad b = \left(\frac{2}{L}\right)^2 (R_{max}^2 - R_{min}^2) \tag{25}$$

Therefore, Equation 11 becomes

$$p = 2\kappa\rho Q \int_{x=0}^{L/2} \frac{dx}{A^2} = 2\kappa\rho Q \int_{x=0}^{L/2} \frac{dx}{\pi^2\left(a+bx^2\right)^2} \tag{26}$$

$$= \frac{2\kappa\rho Q}{\pi^2} \left[\frac{x}{2a(a+bx^2)} + \frac{\arctan(x\sqrt{b/a})}{2a\sqrt{ab}} \right]_0^{L/2} \tag{27}$$

that is

$$p = \frac{\kappa \rho Q L}{2\pi^2} \left[\frac{1}{R_{min}^2 R_{max}^2} + \frac{\arctan\left(\sqrt{\frac{R_{max}^2 - R_{min}^2}{R_{min}^2}}\right)}{R_{min}^3 \sqrt{R_{max}^2 - R_{min}^2}} \right] \tag{28}$$

1.4   Hyperbolic Cosine Tube

For a tube of hyperbolic cosine profile, similar to the profile in Figure 3, the radius is given by

$$r(x) = a\cosh(bx) \qquad -L/2 \le x \le L/2 \tag{29}$$

where

$$a = R_{min} \qquad \text{and} \qquad b = \frac{2}{L}\text{arccosh}\left(\frac{R_{max}}{R_{min}}\right) \tag{30}$$

Hence, Equation 11 becomes

$$p = 2\kappa \rho Q \int_{x=0}^{L/2} \frac{dx}{A^2} = 2\kappa \rho Q \int_{x=0}^{L/2} \frac{dx}{\pi^2 a^4 \cosh^4(bx)} \tag{31}$$

$$= \frac{2\kappa \rho Q}{\pi^2} \left[\frac{\tanh(bx)\left[\text{sech}^2(bx) + 2\right]}{3a^4 b} \right]_0^{L/2} \tag{32}$$

that is

$$p = \frac{\kappa \rho Q L}{3\pi^2} \left[\frac{\tanh\left(\text{arccosh}\left(\frac{R_{max}}{R_{min}}\right)\right)\left[\text{sech}^2\left(\text{arccosh}\left(\frac{R_{max}}{R_{min}}\right)\right) + 2\right]}{R_{min}^4 \qquad \qquad \text{arccosh}\left(\frac{R_{max}}{R_{min}}\right)} \right] \tag{33}$$

1.5   Sinusoidal Tube

For a tube of sinusoidal profile, depicted in Figure 4, where the tube length L spans one complete wavelength, the radius is given by
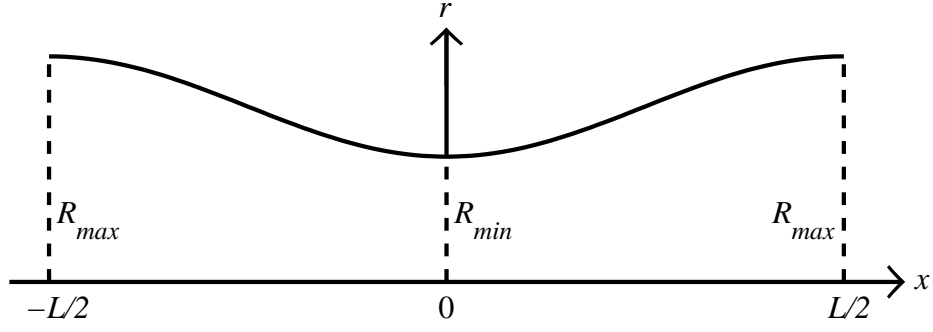
Figure 4: Schematic representation of the radius of a converging-diverging capillary with a sinusoidal profile as a function of the distance along the tube axis.

$$r(x) = a - b\cos(kx) \qquad -L/2 \le x \le L/2 \qquad a > b > 0 \tag{34}$$

where

$$a = \frac{R_{max} + R_{min}}{2} \qquad b = \frac{R_{max} - R_{min}}{2} \qquad \& \qquad k = \frac{2\pi}{L} \tag{35}$$

Hence, Equation 11 becomes

$$p = 2\kappa\rho Q \int_{x=0}^{L/2} \frac{dx}{A^2} = 2\kappa\rho Q \int_{x=0}^{L/2} \frac{dx}{\pi^2 \left[a - b\cos(kx)\right]^4} \tag{36}$$

On performing this integration, the following relation is obtained

$$p = \frac{2\kappa\rho Q}{\pi^2 b^4 k} \left[I\right]_0^{L/2} \tag{37}$$

where

$$
\begin{aligned}
I \; = \; & \frac{(6B^3 + 9B)}{3(B^2 - 1)^{7/2}} \arctan\left(\frac{(B - 1)\tan(\frac{kx}{2})}{\sqrt{B^2 - 1}}\right) - \frac{(11B^2 + 4)\sin(kx)}{6(B^2 - 1)^3[B + \cos(kx)]} \\
& - \frac{5B\sin(kx)}{6(B^2 - 1)^2[B + \cos(kx)]^2} - \frac{\sin(kx)}{3(B^2 - 1)[B + \cos(kx)]^3}
\end{aligned}
\tag{38}
$$

$$\& \qquad B = \frac{R_{max} + R_{min}}{R_{min} - R_{max}} \tag{39}$$

On taking $\lim_{x \to \frac{L}{2}^-} I$ the following expression is obtained

$$p = \frac{2\kappa\rho Q}{\pi^2 b^4 k} \left[-\frac{(6B^3 + 9B)}{3(B^2 - 1)^{7/2}} \frac{\pi}{2} \right] = -\frac{\kappa\rho Q(6B^3 + 9B)}{3\pi b^4 k(B^2 - 1)^{7/2}} \tag{40}$$

Since $B < -1$, $p > 0$ as it should be. On substituting for B, b and k in the last expression we obtain

$$p = \frac{\kappa\rho QL \left(R_{max} - R_{min}\right)^3 \left[2\left(\frac{R_{max}+R_{min}}{R_{max}-R_{min}}\right)^3 + 3\left(\frac{R_{max}+R_{min}}{R_{max}-R_{min}}\right) \right]}{16\pi^2 \left(R_{max} R_{min}\right)^{7/2}} \tag{41}$$

It is noteworthy that all these relations (i.e. Equations 18, 23, 28, 33 and 41), are dimensionally consistent.

2   Validation

The derived converging-diverging formulae (Equations 18, 23, 28, 33 and 41) have been validated by three different ways: comparison to previously-derived formulae based on lubrication approximation, numerical integration, and testing the convergence behavior of the analytical solutions in the limiting cases where the converging-diverging geometries approach a straight tube geometry. These validation methods are outlined in the following subsections.

2.1   Comparison to Lubrication Formulae

For $\alpha = 4/3$, the derived five relations are identical to the previously-derived expressions using the lubrication approximation (refer to Table 1). Since $\alpha = 4/3$ corresponds to a fully-developed parabolic velocity profile (Poiseuille flow), the

lubrication approximation formulae are special cases of the more general 1D Navier-Stokes relations which can accommodate other velocity profiles, such as flat profile (plug flow) when α approaches unity [27, 29, 33, 34, 37, 41].

Table 1: Lubrication approximation table. These formulae are derived in [26].

Conical	$p = \frac{8LQ\mu}{3\pi(R_{max}-R_{min})}\left(\frac{1}{R_{min}^3} - \frac{1}{R_{max}^3}\right)$
Parabolic	$p = \frac{4LQ\mu}{\pi}\left(\frac{1}{3R_{min}R_{max}^3} + \frac{5}{12R_{min}^2R_{max}^2} + \frac{5}{8R_{min}^3R_{max}} + \frac{5\arctan\left(\sqrt{\frac{R_{max}-R_{min}}{R_{min}}}\right)}{8R_{min}^{7/2}\sqrt{R_{max}-R_{min}}}\right)$
Hyperbolic	$p = \frac{4LQ\mu}{\pi}\left(\frac{1}{R_{min}^2R_{max}^2} + \frac{\arctan\left(\sqrt{\frac{R_{max}^2-R_{min}^2}{R_{min}^2}}\right)}{R_{min}^3\sqrt{R_{max}^2-R_{min}^2}}\right)$
Hyperbolic Cosine	$p = \frac{8LQ\mu}{3\pi R_{min}^4}\left(\frac{\tanh\left(\text{arccosh}\left(\frac{R_{max}}{R_{min}}\right)\right)\left\{\text{sech}^2\left(\text{arccosh}\left(\frac{R_{max}}{R_{min}}\right)\right)+2\right\}}{\text{arccosh}\left(\frac{R_{max}}{R_{min}}\right)}\right)$
Sinusoidal	$p = \frac{LQ\mu\left\{2(R_{max}+R_{min})^3+3(R_{max}+R_{min})(R_{max}-R_{min})^2\right\}}{2\pi(R_{max}R_{min})^{7/2}}$

2.2 Numerical Integration

The derived converging-diverging formulae have also been validated by comparison to numerical solutions based on numerical integration by discretizing the converging-diverging tubes of these geometries and solving for a Newtonian flow in each element by averaging the radius of that element. This method has been applied to these geometries using diverse sets of fluid, flow and tube parameters which include μ, ρ, p, Q, α, L, R_{min}, and R_{max}. A sample of these numerical validations is presented in Figure 5 for the five geometries using typical parameters. As seen, the numerical solutions converge to the analytical solutions fairly quickly in all cases. The two solutions become virtually identical for a typical meshing of 40–50 elements. The qualitative difference in convergence behavior between the conical and sinusoidal on one hand and the other geometries on the other hand seems to arise from the converging-diverging nature of these geometries and how gradually it takes place over the tube length. These two types of observed conver-

gence behavior (i.e. oscillatory like conical and asymptotic like parabolic) occur in various numerical contexts and have been observed in different numerical implementations by the author and by other researchers. Another remark is that the convergence rate indicates the quality of the average radius as an indicator of the effective radius of the element. The rapid convergence of the sinusoidal tube may support this guess as the smoothness of the sinusoidal profile makes the average radius very good representative of the effective radius of the discretized sinusoidal segments.

2.3 Convergence to Straight Tube Solution

For $\alpha = 4/3$ (parabolic velocity profile) the sinusoidal equation reduces to the Poiseuille expression when $R_{max} = R_{min}$. With regard to the other geometries, despite the fact that the other four equations are not defined when $R_{max} = R_{min}$, they converge to the Poiseuille value as R_{max} approaches R_{min}, and hence for all practical purposes they are numerically identical to the Poiseuille value when the difference between the two radii is negligible.

(a) Conical

(b) Parabolic
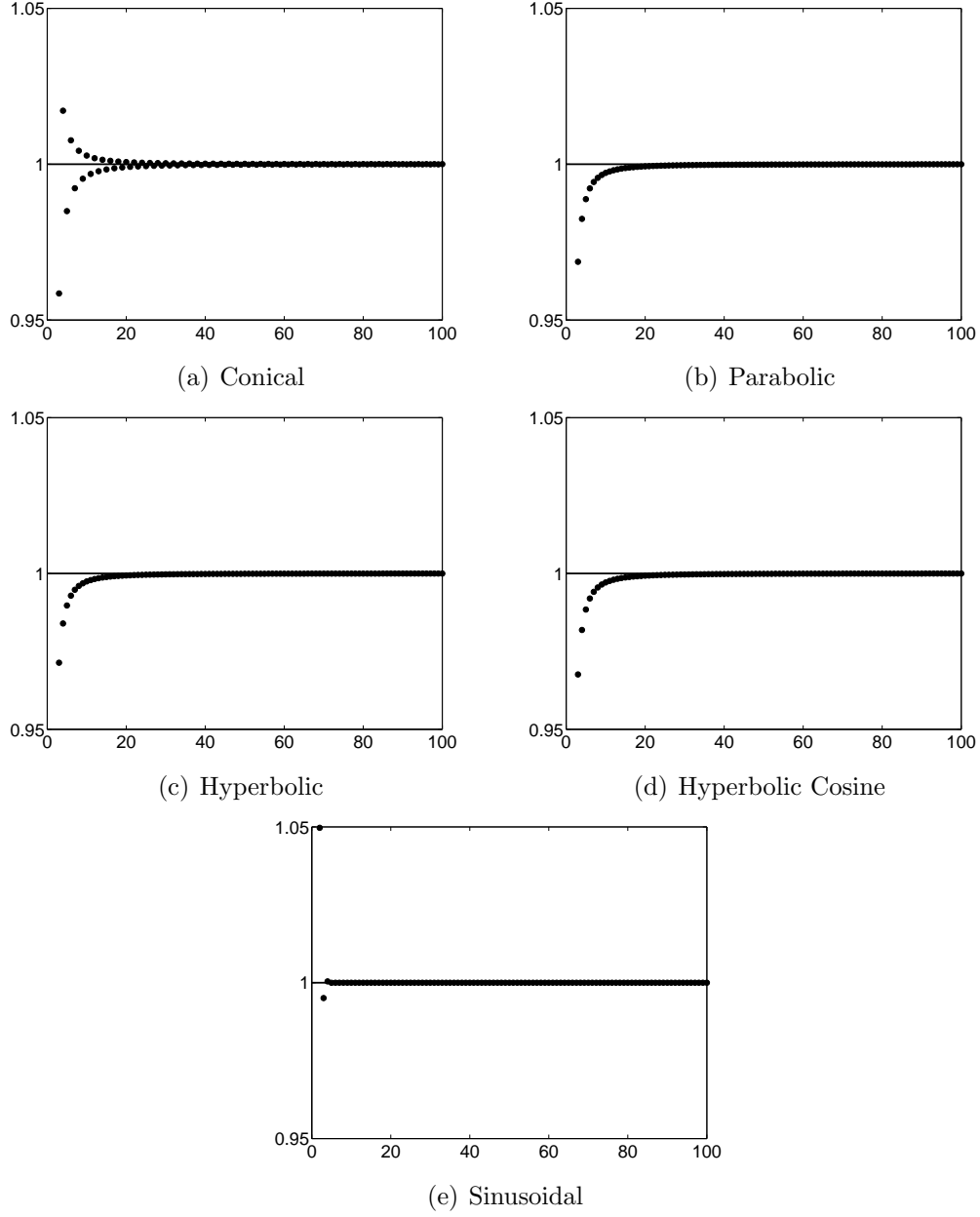
(c) Hyperbolic

(d) Hyperbolic Cosine

(e) Sinusoidal

Figure 5: The ratio of numeric to analytic solutions (y-axis) as a function of the number of discretization elements (x-axis) for the five converging-diverging geometries using typical values for the flow, fluid and capillary parameters. Similar convergence behavior has been observed for other sets of parameters.

3 Conclusions

In this paper we derived analytical expressions relating the pressure drop to the volumetric flow rate for Newtonian fluids in five different converging-diverging geometries using the one-dimensional Navier-Stokes flow equations in axisymmetric rigid tubes. The results obtained in this paper are identical, within a non-dimensional numerical factor, to those derived in [26] using the lubrication approximation. The results have also been validated numerically by comparing the analytical solutions to numerical results obtained from numerical integration for a wide range of flow, fluid and tube characteristics. Moreover, they have been endorsed by testing the convergence behavior of the analytical solutions as the converging-diverging geometries approach the limiting case of a straight tube geometry when $R_{max} \rightarrow R_{min}$.

These expressions can be used in various practical scientific and engineering situations to describe isothermal, uniform, laminar, time-independent flow of incompressible Newtonian fluids through converging-diverging flow paths. These situations include the flow in corrugated vessels and the flow in the pores and throats of porous media where the converging-diverging nature can be idealized by these relatively-simple geometries. The analytical method can also be used to derive expressions for geometries other than those presented in this paper.

Nomenclature

α correction factor for axial momentum flux

κ viscosity friction coefficient ($\text{m}^2.\text{s}^{-1}$)

μ fluid dynamic viscosity (Pa.s)

ρ fluid mass density ($\text{kg}.\text{m}^{-3}$)

A tube cross sectional area (m^2)

L tube length (m)

p pressure (Pa)

Q volumetric flow rate ($\text{m}^3.\text{s}^{-1}$)

r tube radius (m)

R_{max} maximum radius of converging-diverging tube (m)

R_{min} minimum radius of converging-diverging tube (m)

t time (s)

u local axial fluid speed ($\text{m}.\text{s}^{-1}$)

$\overline{u}$ mean axial fluid speed ($\text{m}.\text{s}^{-1}$)

x axial coordinate (m)

References

[1] T. Sochi; M.J. Blunt. Pore-scale network modeling of Ellis and Herschel-Bulkley fluids. *Journal of Petroleum Science and Engineering*, 60(2):105–124, 2008. 5

[2] T. Sochi. Pore-scale modeling of viscoelastic flow in porous media using a Bautista-Manero fluid. *International Journal of Heat and Fluid Flow*, 30(6):1202–1217, 2009. 5

[3] T. Sochi. Non-Newtonian Flow in Porous Media. *Polymer*, 51(22):5007–5023, 2010. 5

[4] T. Sochi. Modelling the Flow of Yield-Stress Fluids in Porous Media. *Transport in Porous Media*, 85(2):489–503, 2010. 5

[5] T. Sochi. Computational Techniques for Modeling Non-Newtonian Flow in Porous Media. *International Journal of Modeling, Simulation, and Scientific Computing*, 1(2):239–256, 2010. 5

[6] T. Sochi. Flow of Non-Newtonian Fluids in Porous Media. *Journal of Polymer Science Part B*, 48(23):2437–2467, 2010. 5

[7] T. Sochi. The flow of power-law fluids in axisymmetric corrugated tubes. *Journal of Petroleum Science and Engineering*, 78(3-4):582–585, 2011. 5

[8] T. Sochi. Slip at Fluid-Solid Interface. *Polymer Reviews*, 51:1–33, 2011. 5

[9] F.M. White. *Viscous Fluid Flow*. McGraw Hill Inc., second edition, 1991. 5

[10] S. Sisavath; X. Jing; R.W. Zimmerman. Laminar Flow Through Irregularly-Shaped Pores in Sedimentary Rocks. *Transport in Porous Media*, 45(1):41–62, 2001. 5

[11] W. Kozicki; C.H. Chou; C. Tiu. Non-Newtonian flow in ducts of arbitrary cross-sectional shape. *Chemical Engineering Science*, 21(8):665–679, 1966. 5

[12] C. Miller. Predicting Non-Newtonian Flow Behavior in Ducts of Unusual Cross Section. *Industrial & Engineering Chemistry Fundamentals*, 11(4):524–528, 1972. 5

[13] S. Oka. Pressure development in a non-Newtonian flow through a tapered tube. *Rheologica Acta*, 12(2):224–227, 1973. 5

[14] E.W. Williams; S.H. Javadpour. The flow of an elastico-viscous liquid in an axisymmetric pipe of slowly varying cross-section. *Journal of Non-Newtonian Fluid Mechanics*, 7(2-3):171–188, 1980. 5

[15] N. Phan-Thien; C.J. Goh; M.B. Bush. Viscous flow through corrugated tube by boundary element method. *Journal of Applied Mathematics and Physics (ZAMP)*, 36(3):475–480, 1985. 5

[16] N. Phan-Thien; M.M.K. Khan. Flow of an Oldroyd-type fluid through a sinusoidally corrugated tube. *Journal of Non-Newtonian Fluid Mechanics*, 24(2):203–220, 1987. 5

[17] A. Lahbabi; H-C. Chang. Flow in periodically constricted tubes: Transition to inertial and nonsteady flows. *Chemical Engineering Science*, 41(10):2487–2505, 1986. 5

[18] S.R. Burdette; P.J. Coates; R.C. Armstrong; R.A. Brown. Calculations of viscoelastic flow through an axisymmetric corrugated tube using the explicitly elliptic momentum equation formulation (EEME). *Journal of Non-Newtonian Fluid Mechanics*, 33(1):1–23, 1989. 5

[19] S. Pilitsis; A. Souvaliotis; A.N. Beris. Viscoelastic flow in a periodically constricted tube: The combined effect of inertia, shear thinning, and elasticity. *Journal of Rheology*, 35(4):605–646, 1991. 5

[20] S. Pilitsis; A.N. Beris. Calculations of steady-state viscoelastic flow in an undulating tube. *Journal of Non-Newtonian Fluid Mechanics*, 31(3):231–287, 1989. 5

[21] D.F. James; N. Phan-Thien; M.M.K. Khan; A.N. Beris; S. Pilitsis. Flow of test fluid M1 in corrugated tubes. *Journal of Non-Newtonian Fluid Mechanics*, 35(2-3):405–412, 1990. 5

[22] K.K. Talwar; B. Khomami. Application of higher order finite element methods to viscoelastic flow in porous media. *Journal of Rheology*, 36(7):1377–1416, 1992. 5

[23] T. Koshiba; N. Mori; K. Nakamura; S. Sugiyama. Measurement of pressure loss and observation of the flow field in viscoelastic flow through an undulating channel. *Journal of Rheology*, 44(1):65–78, 2000. 5

[24] S.H. Momeni-Masuleh; T.N. Phillips. Viscoelastic flow in an undulating tube using spectral methods. *Computers & fluids*, 33(8):1075–1095, 2004. 5

[25] D. Davidson; G.L. Lehmann; E.J. Cotts. Horizontal capillary flow of a Newtonian liquid in a narrow gap between a plane wall and a sinusoidal wall. *Fluid Dynamics Research*, 40(11-12):779–802, 2008. 5

[26] T. Sochi. The Flow of Newtonian Fluids in Axisymmetric Corrugated Tubes. 2010. arXiv:1006.1515v1. 5, 14, 17

[27] L. Formaggia; J.F. Gerbeau; F. Nobile; A. Quarteroni. On the coupling of 3D and 1D Navier-Stokes equations for flow problems in compliant vessels.

Computer Methods in Applied Mechanics and Engineering, 191(6-7):561–582, 2001. 6, 14

[28] W. Ruan; M.E. Clark; M. Zhao; A. Curcio. A Hyperbolic System of Equations of Blood Flow in an Arterial Network. *SIAM Journal on Applied Mathematics*, 64(2):637–667, 2003. 6

[29] S.J. Sherwin; V. Franke; J. Peiró; K. Parker. One-dimensional modelling of a vascular network in space-time variables. *Journal of Engineering Mathematics*, 47(3-4):217–250, 2003. 6, 14

[30] S. Urquiza; P. Blanco; G. Lombera; M. Venere; R. Feijoo. Coupling Multidimensional Compliant Models For Carotid Artery Blood Flow. *Mecánica Computacional*, XXII(3):232–243, 2003. 6

[31] V. Mili šić; A. Quarteroni. Analysis of lumped parameter models for blood flow simulations and their relation with 1D models. *Mathematical Modelling and Numerical Analysis*, 38(4):613–632, 2004. 6

[32] M.Á. Fernández; V. Mili šić; A. Quarteroni. Analysis of a Geometrical Multiscale Blood Flow Model Based on the Coupling of ODEs and Hyperbolic PDEs. *Multiscale Modeling & Simulation*, 4(1):215–236, 2005. 6

[33] L. Formaggia; D. Lamponi; M. Tuveri; A. Veneziani. Numerical modeling of 1D arterial networks coupled with a lumped parameters description of the heart. *Computer Methods in Biomechanics and Biomedical Engineering*, 9(5):273–288, 2006. 6, 14

[34] L. Formaggia; A. Moura; F. Nobile. Coupling 3D and 1D fluid-structure interaction models for blood flow simulations. *Proceedings in Applied Mathematics and Mechanics, Special Issue: GAMM Annual Meeting 2006 - Berlin*, 6(1):27–30, 2006. 6, 14

[35] J. Alastruey; S.M. Moore; K.H. Parker; T. David; J. Peiró S.J. Sherwin. Reduced modelling of blood flow in the cerebral circulation: Coupling 1-D, 0-D and cerebral auto-regulation models. *International Journal for Numerical Methods in Fluids*, 56(8):1061–1067, 2008. 6

[36] J. Alastruey; K.H. Parker; J. Peiró; S.J. Sherwin. Lumped parameter outflow models for 1-D blood flow simulations: Effect on pulse waves and parameter estimation. *Communications in Computational Physics*, 4(2):317–336, 2008. 6

[37] J. Lee; N. Smith. Development and application of a one-dimensional blood flow model for microvascular networks. *Proceedings of the Institution of Mechanical Engineers, Part H: Journal of Engineering in Medicine*, 222(4):487–512, 2008. 6, 14

[38] T. Passerini; M. de Luca; L. Formaggia; A. Quarteroni; A. Veneziani. A 3D/1D geometrical multiscale model of cerebral vasculature. *Journal of Engineering Mathematics*, 64(4):319–330, 2009. 6

[39] J. Janela; A.B. de Moura; A. Sequeira. Comparing Absorbing Boundary Conditions for a 3D Non Newtonian Fluid-Structure Interaction Model for Blood Flow in Arteries. *Mecánica Computacional*, XXIX(59):5961–5971, 2010. 6

[40] L. Formaggia; D. Lamponi; A. Quarteroni. One-dimensional models for blood flow in arteries. *Journal of Engineering Mathematics*, 47(3/4):251–276, 2003. 6

[41] N.P. Smith; A.J. Pullan; P.J. Hunter. An Anatomically Based Model of Transient Coronary Blood Flow in the Heart. *SIAM Journal on Applied Mathematics*, 62(3):990–1018, 2002. 14